Miner Deposita (2017) 52:675–686
DOI 10.1007/s00126-016-0691-7

ARTICLE

Cadmium isotope fractionation in the Fule Mississippi Valley-type deposit, Southwest China

Chuanwei Zhu[1] · Hanjie Wen[1] · Yuxu Zhang[1] · Shaohong Fu[1] · Haifeng Fan[1] · Christophe Cloquet[2]

Received: 22 November 2015 / Accepted: 6 October 2016 / Published online: 9 November 2016

Abstract High-precision cadmium (Cd) isotope compositions are reported for sphalerite, galena, and smithsonite from the Fule Zn–Pb–Cd deposit, a typical Mississippi Valley-type deposit in Southwest China. Dark sphalerite has lighter $\delta^{114/110}$Cd values (0.06 to 0.46 ‰) than light sphalerite (0.43 to 0.70 ‰), and the Cd in galena is primarily in the form of sphalerite micro-inclusions with $\delta^{114/110}$Cd of −0.35 to 0.39 ‰. From early to late stages, $\delta^{114/110}$Cd values of smithsonite regularly increase from 0.19 to 0.42 ‰, whereas Cd/Zn ratios decrease from 252 to 136; the $\delta^{114/110}$Cd variation pattern of supergene smithsonite reflects kinetic Rayleigh fractionation during low-temperature processes. From the bottom to the top of the orebody, the dark sphalerite has different patterns in $\delta^{114/110}$Cd values, Cd/Zn ratios, δ^{34}S values, and Fe concentrations compared to the light sphalerite, indicating that dark and light sphalerite formed by different processes. The varying patterns of $\delta^{144/110}$Cd values and Cd/Zn ratios within light sphalerite are similar to those of layered smithsonite, and the $\delta^{144/110}$Cd values have a positive correlation with δ^{34}S values, indicating that Cd isotope fractionation in the light sphalerite was due to kinetic Rayleigh fractionation. Instead, in dark sphalerite, the $\delta^{144/110}$Cd values have a negative correlation with δ^{34}S values and a positive correlation with the Cd/Zn ratio. Thus, it can be concluded that dark sphalerite could be modeled in terms of two-component mixing (basement fluid and host-rock fluid), which is in agreement with previous explanations for the negative correlation between δ^{66}Zn and δ^{34}S in some typical Zn–Pb deposits. We propose that the significant variation in Cd isotope composition observed in the Fule Zn–Pb–Cd deposit confirms that Cd isotopes can be used for tracing fluid evolution and ore formation.

Keywords Cadmium and sulfur isotopes · Cd-bearing minerals · Zn–Pb–Cd deposits · Stable isotope fractionation

Editorial handling: B. Lehmann

✉ Hanjie Wen
wenhanjie@vip.gyig.ac.cn

[1] State Key Laboratory of Ore Deposit Geochemistry, Institute of Geochemistry, Chinese Academy of Sciences, Guiyang 550081, China

[2] Centre de Recherches Petrographique et Geochimiques, CNRS/UMR 7358, 15,Rue Notre-Dame-Pauvres, B. P. 20, 54501 Vandoeuvre-les-Nancy Cedex, France

Introduction

Cadmium (Cd) is a chalcophile trace element with a crustal abundance of approximately 0.08 ppm (Rudnick and Gao 2003). Because of its low concentration and the rarity of its independent minerals, Cd ore deposits are rare. Instead, Cd occurs primarily as an associated minor element in Zn–Pb ore deposits, and is primarily hosted in sphalerite as isomorphic impurity with a typical mean of 0.2–3.0 wt% Cd (Schwartz 2000; Cook et al. 2009; Ye et al. 2011; Zhu et al. 2013). Sediment-hosted Zn–Pb deposits are the major source of industrially utilized cadmium, of which the Mississippi Valley-type (MVT) deposits are the most important.

In the past decades, new advances in Cd isotope systematics have been made in terms of (1) modern analytical techniques applied to a variety of geological materials (Wombacher et al. 2003; Cloquet et al. 2006; Ripperger et al. 2007; Schmitt et al. 2009; Zhu et al. 2013, 2015, 2016; Lambelet et al. 2013; Wen et al. 2015, 2016) and (2) theoretical prediction and experimental studies on Cd isotope fractionation (Horner et al. 2011; Yang et al. 2014; Zhang et al.

2016). Recently, our Cd isotope study on the hydrothermal Tianbaoshan deposit shows that the variations of $\delta^{114/110}$Cd values in sulfides have no correlation with fluid temperature (Zhu et al. 2016); however, different types of Zn–Pb deposits have various characteristics in Cd concentrations and isotope signatures, indicating different ore formation types (Wen et al. 2016). These studies have revealed significant Cd isotope fractionation and also provided a possibility of using Cd isotopes as a new geochemical tracer.

We here investigated the Cd and S isotope composition of the Fule deposit in SW China. This deposit is a typical MVT Zn–Pb–Cd ore deposit in the southeastern part of the Sichuan–Yunnan–Guizhou (SYG) metallogenic province (Fig. 1). The spatial and temporal variations of Cd and S isotopes in the hydrothermal system provide a better understanding for the Cd and S isotope fractionation during the hydrothermal processes of ore formations. Furthermore, the Cd isotope variations in layered smithsonite record progressive crystallization at a fine scale similar to sphalerite from low-temperature fractionation processes (Gagnevin et al. 2012).

Geological setting

In the Fule mining area, the stratigraphic sequence comprises Permian and Upper Triassic strata (Fig. 2a). The Lower Permian Maokou Formation (P_{1m}) is the principal ore-hosting sequence and predominantly comprises gray (dark to light gray) dolomitic limestone and green–gray flint-nodule-containing limestone intercalated with dolostone. All of these are overlain by Middle Permian Emeishan flood basalts (Emeishan Formation, $P_2\beta$). The Emeishan basalts are in turn

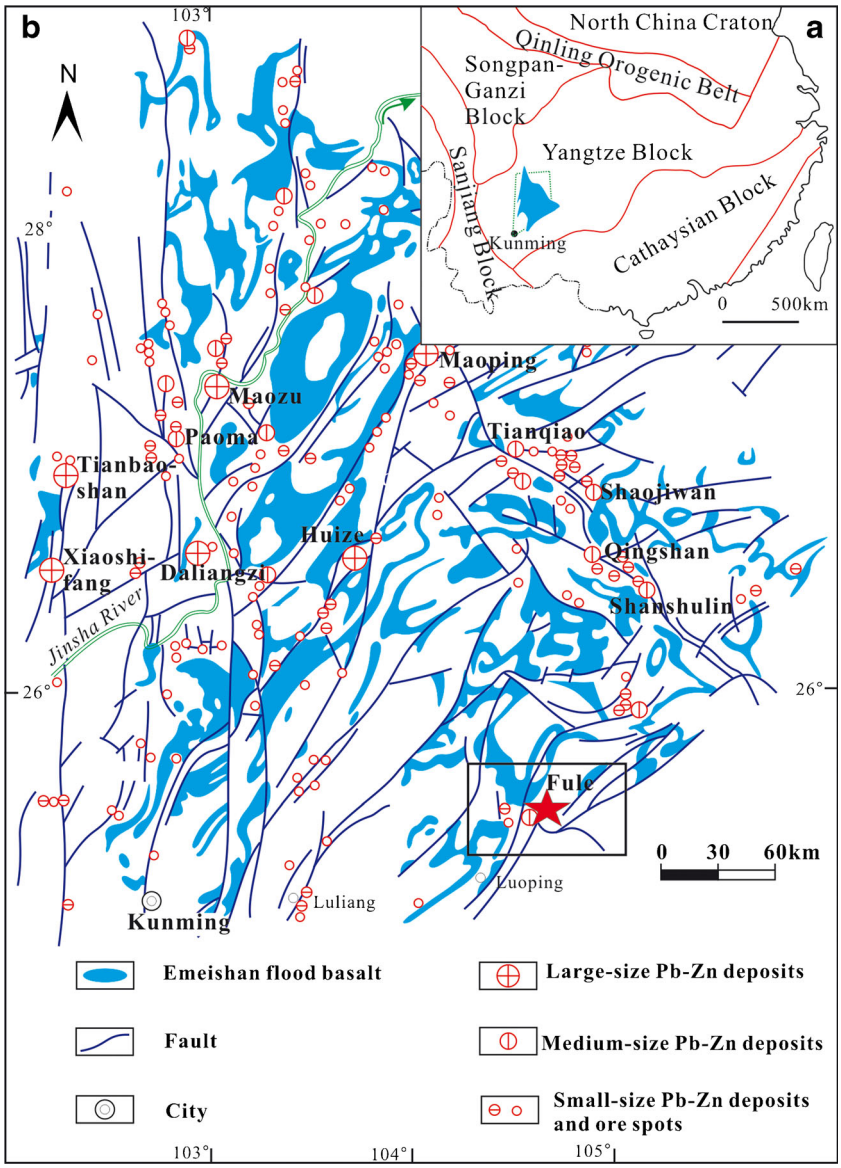

Fig. 1 *A* Sketch of the tectonic framework of South China; *B* Map of the Sichuan–Yunnan–Guizhou metallogenic province, SW China, showing the distribution of the Emeishan flood basalts, major faults, and Zn–Pb ore deposits. Modified from Zhou et al. (2013)

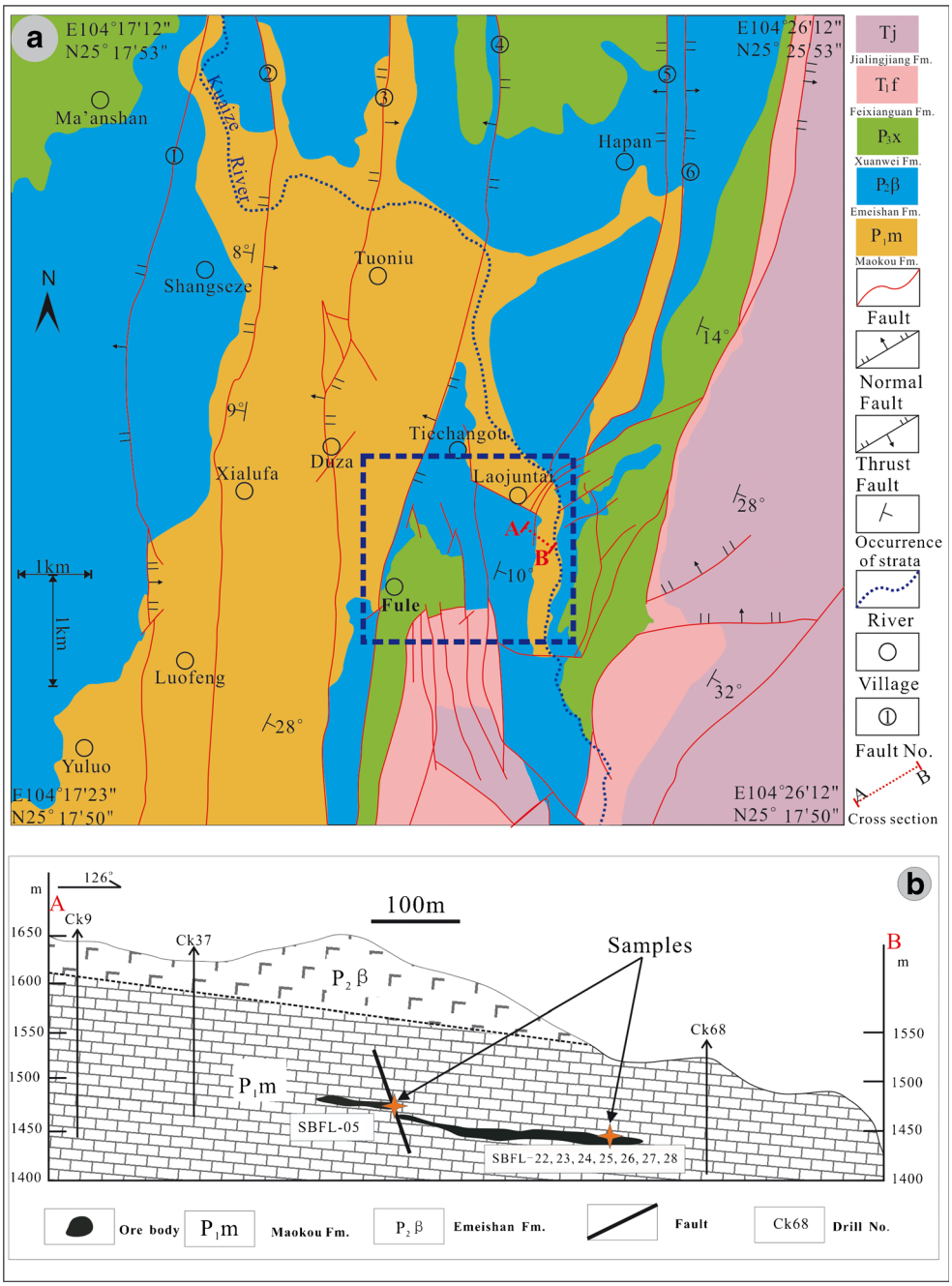

Fig. 2 **a** Regional geological map and **b** cross section of the Fule deposit (modified after data up to 1994 from the Fule mine)

overlain by Upper Permian sandstone, siltstone, and coal measures (Xuanwei Formation, P_{3x}). The Triassic strata comprise siltstone, sandstone, shale, dolomitic limestone, and limestone (Feixianguan Formation,T_{1f}, Jialingjiang Formation, T_j). Two fault systems are present in the area, namely, NS- and NE-trending faults, all of which formed post-ore (Fig. 2).

The demonstrated reserves in the Fule deposit are 2.7 Mt Zn ore and 58.8 Mt Pb ore at grades of 4.5 % Zn and 0.55 % Pb, respectively. In addition, the zinc ores contain proven reserves of approximately 4567 t Cd, 329 t Ge, and 177 t Ga at grades of 0.127 wt% Cd, 0.012 wt% Ge, and 0.007 wt% Ga, respectively (Si 2005). The geological features of the Fule deposit were summarized by Si (2005). Approximately 20 orebodies of various sizes are present within an area about 3 km long and 1.5 km wide. The orebodies are stratabound and lenticular in shape and locally pinch and swell. They strike 130–140° NW and dip 5–15° SE, somewhat parallel to the bedding of the host rocks (Fig. 2b). The ores in the Fule deposit are dominantly sulfide ores, with small amounts of oxidized ores near the surface and faults.

Detailed field and microscopic observations indicate that the mineralogy is relatively simple and mainly includes

sphalerite, pyrite, galena, calcite, and dolomite. The major ore minerals are sphalerite and galena, associated with minor pyrite, tetrahedrite, chalcocite, and smithsonite. Gangue minerals are primarily dolomite and calcite with minor barite and gypsum. The ores are divided into four major types on the basis of their structure and texture: brecciated ore (including sphalerite and sphalerite–galena; Fig. 3a, b), massive ore (including sphalerite, galena, sphalerite–galena, and smithsonite), spotted ore (including sphalerite and galena), and layered ore (smithsonite dominant; Fig. 3f), of which brecciated ore is the dominant type. The principal ore minerals are subhedral–euhedral granular and intergrown (Fig. 3b–e). Microcrystalline to coarsely crystalline granular textures and euhedral–subhedral–anhedral granular textures are the most common. The ore structures are dominated by brecciated accumulations of sulfide minerals, but may be veined, disseminated, spotted, and massive. The mineralization has been divided into three stages (Si 2005), which are (1) sedimentary diagenetic stage, including sedimentary pyrite in host carbonate rocks; (2) hydrothermal ore-forming stage, including sphalerite, galena, pyrite, dolomite, and calcite; and (3) supergene stage, including smithsonite, barite, and gypsum.

Sphalerite is present as fine- to macro-crystalline, euhedral to anhedral, and granular (0.1–10 mm). Several formation stages of sphalerite within a hand specimen can be identified on the basis of the mineral paragenesis, textural and structural characteristics, and crosscutting relations. In general, dark sphalerite has an impregnated structure and is surrounded by light sphalerite (Fig. 3b, c), confirming that the dark sphalerite was formed earlier than the light one (Si 2005; Han et al. 2007). Sphalerite is present in brecciated, massive, banded, and disseminated aggregates co-existing with galena, pyrite, dolomite, and calcite. Galena is fine- to macro-crystalline, euhedral to subhedral, or subhedral to anhedral with grain sizes of 1–30 mm. Stress deformation and euhedral textures are common. Galena contains micro-inclusions of sphalerite (Fig. 3d, e). Pyrite is microcrystalline and anhedral. Smithsonite can easily be distinguished and has a layered and botryoidal structure (Fig. 3f). Dolomite is present as coarse-grained crystals, 1–3 mm in size, which occur in euhedral–subhedral granular aggregates, primarily visible in massive and banded aggregates, as well as veinlets within the orebodies (Fig. 3a). Calcite mainly occurs in dolomite and sometimes on veinlets within massive sphalerite and galena.

Samples and methods

The sampling locations within the orebody are shown in Fig. 2b. Seven representative primary ore samples were taken from the bottom to the top of the no. 78 ore body over a vertical length of about 60 cm (Fig. 4; Table 1). On the basis of the clear boundaries between the seven samples associated with variable mineral paragenesis, and the textural and structural characteristics, we conclude that the bottom samples formed earlier than the top ones (Fig. 4; Table 1).

Dark and light sphalerite and galena separates (40–60 mesh) from these ore samples were handpicked under a binocular microscope. Samples SBFL-24 and SBFL-26 (both dark sphalerite) were selected as parallel samples to investigate whether the distribution of Cd isotopes was homogeneous in a hand specimen. Layered smithsonite was sampled

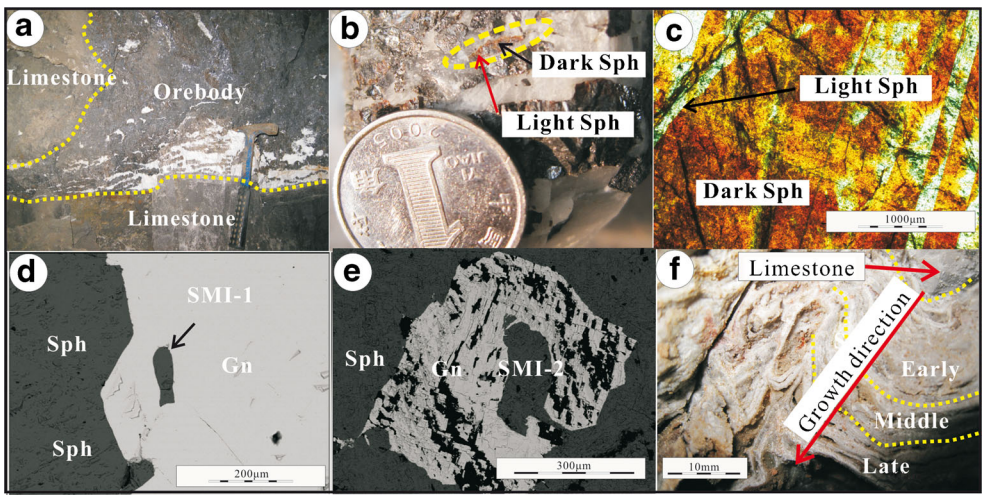

Fig. 3 Field photographs (**a**, **b**, and **f**) from the underground workings of the Fule deposit along with a transmitted light microphotograph (**c**) and two back-scattered electron images (**d** and **e**) of sphalerite. Note: **a** obvious boundaries between the orebody and the dark gray dolomitic limestone wall rock; **b** dark and light sphalerite in a hand specimen: dark sphalerite (*Dark-Sph*) is surrounded by light sphalerite (*Light-Sph*); **c** dark sphalerite cross-cut by light sphalerite; **d** early-stage sphalerite (stage 1 Sph) surrounded by subhedral–euhedral crystalline galena (*Gn*) associated with late-stage sphalerite (stage 2 Sph), sample SBFL-23; **e** subhedral–euhedral crystalline galena replaced by sphalerite micro-inclusions (SMI), sample SBFL-22; **f** distinctive boundaries between layered smithsonite and limestone

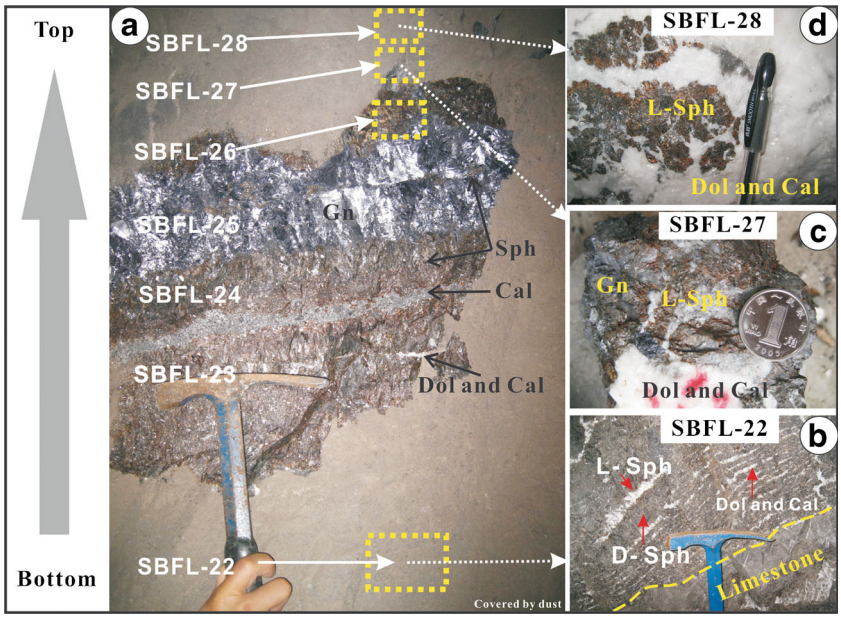

Fig. 4 Photographs of the section of the orebody from which the samples in this study were obtained. *A* Overall view of the orebody; *B–D* close-up images of different parts of the orebody. The *yellow rectangles* indicate the positions of the close-up images within the orebody. *D-Sph* dark sphalerite, *L-Sph* light sphalerite, *Dol* dolomite, *Cal* calcite, *Gn* galena

from early to late mineralization stages in a karst cave (Fig. 3f), and two limestone samples were taken from the Maokou Formation outside the Fule mine.

Prior to chemical analysis, all samples were crushed to less than 200 mesh. For each sample, ~150 mg was weighed out and placed in a Teflon digestion vessel, reacted with 3 mL of concentrated HNO_3 at 110 °C for more than 24 h, and heated to dryness on a hotplate at 110 °C. Each residue was digested with 3 mL of concentrated HF and 3 mL of Milli-Q water, then heated at 110 °C until dryness. Finally, 10 mL of 1 % HNO_3 was added and the solution was transferred into a 15-mL polypropylene centrifuge tube. After centrifugation (4000 r/min, 5 min), 4 mL of the supernatant was transferred for measurement of major- and trace-element concentrations, and another 2 mL of supernatant was transferred for chemical purification. For the limestone samples, ~1 g was weighed out; the detailed digestion methodology of the limestone samples is as reported in our recent work on Mo isotopes (Liu et al. 2016).

Before chemical purification, the 2-mL supernatant was evaporated to dryness at 110 °C followed by addition of 2 mL of 2 N HCl. The supernatant containing Cd and other soluble chlorate complexes was loaded into an anion-exchange chromatographic column filled with 3 mL of AG–MP–1 M resin (Bio-Rad, Hercules, CA, USA, 100–200 mesh). After adsorption of Cd onto the column, 10 mL of 2 N HCl, 30 mL of 0.3 N HCl (elute), 20 mL of 0.06 N HCl, and 5 mL of 0.012 N HCl were passed in sequence through the column to elute the remaining matrix (Zhu et al. 2013; Wen et al. 2015; Zhang et al. 2016). This methodology is similar to that of Pallavicini et al. (2014). The column was then eluted with 20 mL of 0.0012 N HCl for Cd, and the leachate was evaporated to dryness at 110 °C. After

Table 1 A sampling list for different ores from bottom to top of the studied orebody

Sample no.	Positions	Object	Major characteristics of ores
SBFL-28	Top	Light Sph and Gn	Spotted ores, subhedral–euhedral crystalline Gn and Sph embraced by dolomite and calcite
SBFL-27	↑	Light Sph and Gn	Spotted ores, massive Sph embraced by dolomite
SBFL-26		Dark Sph; Gn and light Sph minor	Massive ores, primarily consist of Sph, Gn is minor
SBFL-25		Dark Sph; Gn and light Sph minor	Massive ores, primarily consist of Gn, Sph is minor
SBFL-24		Dark Sph; Gn and light Sph minor	Massive ores, primarily consist of Sph, Gn exhibiting as band
SBFL-23		Dark Sph; Gn and light Sph minor	Massive ores, primarily consist of Sph, Gn exhibiting as spots
SBFL-22	Bottom	Dark Sph; Gn and light Sph minor	Massive ores, primarily consist of Sph, Gn is minor, dolomite as band

Sph sphalerite, *Gn* galena

evaporation, the residue was dissolved in 3 mL of 1 % HNO_3. One milliliter of the leachate was transferred for elemental measurements (ICP-MS) to monitor interfering matrix elements (e.g., Zn, Sn, In, and Pd) and calculate Cd recovery. The residual solution was subsequently used for isotopic analysis. The method yielded a mean Cd recovery of 99.8 %, and the potentially interfering elements were detected at concentrations that were negligible relative to that of Cd (Wen et al. 2015; Zhang et al. 2016).

Cd, Zn, and Fe concentrations in the ore samples were measured using a Varian Vista MPX ICP-OES, and other trace elements (e.g., Sn and In) were measured using an ELAN DRC-e-type ICP-MS at the State Key Laboratory of Ore Deposit Geochemistry, Institute of Geochemistry, Chinese Academy of Sciences. Solution standards have been selected for the measurement of major (ALSWAT01 and ALSWATx10, Inorganic Ventures, USA) and trace elements (Reicptune33A, Reagecon, Republic of Ireland); the relative deviation and the relative error are less than 10 %. Trace elements in limestone were also analyzed by ICP-MS. Sulfur isotopes were measured using a continuous-flow mass spectrometer at the same institute. The standard reference materials for sulfur isotope measurement were GBW 04415 and GBW 04414 Ag_2S (Chinese National Standards), which yielded a relative error (2σ) of <0.1 ‰. All of the S isotope ratios are reported relative to the Canyon Diablo Troilite (CDT).

Cadmium isotope ratios were measured using a Thermo-Scientific Neptune MC-ICP-MS coupled with CETAC Aridus II at the State Key Laboratory of Ore Deposit Geochemistry, Institute of Geochemistry, Chinese Academy of Sciences. All samples and bracketing reference solutions were run in two blocks with 30 cycles per block. This system typically generated a total Cd signal of approximately 87 V/ppm at an uptake rate of ~100 μL/min. After each run, the membrane desolvation system was rinsed with 5 % HNO_3 until the signal intensity reached the original background level (^{111}Cd <0.001 V).

The standard-sample bracketing method was used to calculate delta values:

$$\delta^{*/110}\mathrm{Cd}\ (‰) = \left[\left({}^{*}\mathrm{Cd}/{}^{110}\mathrm{Cd}\right)_{\mathrm{sample}}/\left(\left({}^{*}\mathrm{Cd}/{}^{110}\mathrm{Cd}\right)_{\mathrm{std}}\right)-1\right] \times 1000,$$

where * denotes the 114, 113, 112, and 111 Cd isotopes and std is the Spex Cd reference standard. The Cd concentrations in samples and a Cd reference standard (Spex Cd standard) were analyzed at the same concentration to within a 10 % difference (Cloquet et al. 2005). Two Cd isotope standards (Münster Cd solution and NIST SRM 3108 Cd solution) were additionally used as second reference standards. The long-term reproducibility of Cd isotope ratios in this laboratory has been reported by Zhang et al. (2016). The measurements of Münster Cd relative to Spex Cd yielded $\delta^{114/110}$Cd = 4.50 ± 0.08 (2SD, N = 31), which is identical to the value reported by Cloquet et al. (2005); the analyses of NIST SRM 3108 Cd relative to Spex Cd yielded $\delta^{114/110}$Cd = 0.11 ± 0.03 ‰ (2SD, N = 30) (Zhang et al. 2016).

The data listed in Table 2 demonstrate that the $\delta^{114/110}$Cd values of three pairs of duplicate samples show good reproducibility, indicating that accidental errors were efficiently avoided during sample preparation and testing. The $\delta^{114/110}\mathrm{Cd}_{\mathrm{spex}}$ vs $\delta^{112/110}\mathrm{Cd}_{\mathrm{spex}}$ diagram (Fig. 5) shows that the Cd isotopic compositions of all samples fall on the equilibrium and theoretical kinetic mass fractionation lines within the errors, as is also the case for the Spex, NIST SRM 3108 Cd, and Münster Cd standards, indicating that isobaric interference was efficiently removed by the chemical purification (matrix interference) and the isobaric interference correction (e.g., Sn interference) during measurement.

Results

The concentrations of Zn, Fe, and Cd in the studied samples are listed in Table 2. The Fule sphalerite samples have 59.4 ± 3.3 wt% Zn (n = 12) on average and mean concentrations of 17,410 ± 9298 ppm Cd (n = 12) and 526 ± 178 ppm Fe (n = 12). Clearly, the Zn contents in sphalerite are slightly lower than that of pure sphalerite (ideal composition 67.1 wt% Zn). This may result from the presence of impurities in sphalerite, possibly in the form of small amounts of other minerals such as galena (Fig. 3e). Considering the contamination by gangue minerals in sphalerite, Cd/Zn ratios (Cd/Zn = Cd (ppm)/Zn(%)) are more suitable to reflect the variations of Cd concentrations in sphalerite. Although the Zn and Cd contents in two pairs of parallel samples (SBFL-24 and SBFL-26; Table 2) are slightly different, the Cd/Zn ratios and $\delta^{114/110}$Cd values of these two pairs of parallel samples are within analytical error, indicating that the distribution of Cd isotopes is homogeneous at least at the hand-specimen scale.

The measured $\delta^{114/110}$Cd values of sphalerite vary from 0.06 to 0.70 ‰, which is different from the range reported for sphalerite of 0.34–0.93 ‰ (Schmitt et al. 2009; Zhu et al. 2013, 2016; Table 2; Fig. 6a). The three pairs of dark and light sphalerite samples SBFL-22, SBFL-23, and SBFL-24 display much higher Cd and Fe concentrations and Cd/Zn ratios in the dark fractions than in the light fractions (Table 2). The Cd contents in galena (micro-inclusions of sphalerite in galena) are much lower than those in sphalerite (Table 2), falling in a range between 48 and 1163 ppm, with a Cd/Zn of 443 ± 279 (n = 6), similar to the sphalerite samples. The $\delta^{114/110}$Cd values of galena are between −0.35 and 0.39 ‰, with a range of 0.74 ‰, similar to the range of sphalerite (0.64 ‰). However, Cd is generally lighter in galena samples than in sphalerite samples, as attested by six sphalerite–galena pairs (SBFL-22, SBFL-23, SBFL-24, SBFL-25, SBFL-27, and SBFL-28; Table 2).

Table 2 Cadmium isotopic variations in sulfides and layered smithsonite

Sample no.	Sample type	Cd (ppm)	Zn (%)	Fe (ppm)	Cd (ppm)/Zn (%) ratios	$\delta^{114/110}$Cd (‰)	2σ (‰)	$\delta^{112/110}$Cd (‰)	2σ (‰)	$\delta^{34}S_{CDT}$ (‰)
SBFL-1	Limestone	0.76	25[a]	1400	304	0.63	0.08	0.30	0.03	
SBFL-2	Limestone	0.60	11[a]	400	545	0.58	0.12	0.27	0.07	
SBFL-22 (D)[b]	Sph	14,714	57.875	970	254	0.06	0.04	0.03	0.01	14.8
SBFL-22 (L)[b]	Sph	9083	62.632	448	145	0.52	0.04	0.26	0.02	14.0
SBFL-23 (D)[b]	Sph	15,046	60.672	706	248	0.28	0.03	0.15	0.01	13.8
SBFL-23 (L)[b]	Sph	13,735	60.912	685	225	0.43	0.04	0.21	0.01	14.0
SBFL-24 (D)[b]	Sph	18,479	55.295	547	334	0.33	0.01	0.17	0.01	12.8
	Parallel	19,532	59.150	450	330	0.29	0.05	0.15	0.01	
SBFL-24 (L)[b]	Sph	16,783	62.500	365	269	0.47	0.01	0.24	0.01	12.3
SBFL-25 (D)[b]	Sph	18,645	51.676	446	361	0.21	0.02	0.10	0.00	13.4
SBFL-26 (D)[b]	Sph	34,981	59.498	395	588	0.46	0.08	0.23	0.04	11.7
	Parallel	34,757	59.352	384	586	0.43	0.03	0.22	0.01	
SBFL-27 (L)[b]	Sph	5238	62.820	424	83	0.70	0.05	0.34	0.01	16.5
SBFL-28 (L)[b]	Sph	7930	60.724	492	131	0.63	0.02	0.31	0.01	15.9
SBFL-22	Gn	1163	2.272		512	−0.35	0.06	−0.16	0.05	12.7
SBFL-23	Gn	601	1.624		370	0.09	0.02	0.05	0.01	10.9
SBFL-24	Gn	48	0.302		159	0.01	0.02	0.00	0.03	9.6
SBFL-25	Gn	135	0.144		938	0.11	0.03	0.05	0.01	10.5
SBFL-27	Gn	122	0.576		212	0.08	0.06	0.04	0.03	13.0
SBFL-28	Gn	135	0.287		470	0.39	0.01	0.21	0.00	10.0
SBFL-05	Sm(Late)	6216	45.719		136	0.42	0.01	0.20	0.01	
	Parallel	6389	44.999		142	0.42	0.01	0.20	0.01	
SBFL-05	Sm(Early)	12,128	48.139		252	0.19	0.01	0.06	0.01	
SBFL-05	Sm(Middle)	6283	44.573		141	0.33	0.04	0.15	0.01	
NIST SRM 3108	Standard					0.11	0.04	0.06	0.02	
Münster	Standard					4.50	0.08	2.25	0.05	

Münster has been measured 31 times and NIST SRM 3108 has been measured 30 times

Sph sphalerite, *Gn* galena, *Sm* smithsonite, *(D)* dark sphalerite, *(L)* light sphalerite

[a] Reported for ppm

[b] Reported by Wen et al. (2016) except for $\delta^{34}S_{CDT}$ values

The two limestone samples have much higher Cd concentrations (~0.68 ppm) than average continental crust, and the $\delta^{114/110}$Cd values vary from 0.60 to 0.76 ‰, which is heavier than average continental crust ($\delta^{114/110}$Cd = 0.05 ± 0.08 ‰, 2SD; Schmitt et al. 2009). From early to late stages, the $\delta^{114/110}$Cd values of smithsonite increase steadily from 0.19 to 0.42 ‰ (Fig. 7), whereas the Cd contents decrease from 12,100 to 6220 ppm (mean 7750 ± 2920 ppm; n = 4; Fig. 7).

Sphalerite has δ^{34}S values ranging from 11.7 to 16.5 ‰, which are heavier than those of galena with 9.6–13.0 ‰ (Table 2; Fig. 6). A good correlation between δ^{34}S and Cd/Zn is observed for ten measurements on sphalerite (R^2 = 0.68; coefficient of determination) (Fig. 6b). This correlation within dark as well as light sphalerite is much better, with R^2 of 0.79 and 0.83, respectively (Fig. 6b).

Discussion

Implication of Cd contents in sulfide and oxidized minerals

Previous studies showed that the range of Cd concentrations in galena from hydrothermal deposits is 10–500 ppm (Schwartz 2000); however, recent studies have reported a positive correlation between Zn and Cd in galena and further argued that both Zn and Cd are presented as sphalerite micro-inclusions in galena (Palero-Fernández and Martín-Izard 2005; Zhou et al. 2011). Our study in the Fule deposit also demonstrated that Cd in galena is likely related to sphalerite micro-inclusions based on the following reasons. First, the Cd contents of six galena samples show a large range (48–1163 ppm); except sample SBFL-25 (Cd/Zn = 938), the Cd/

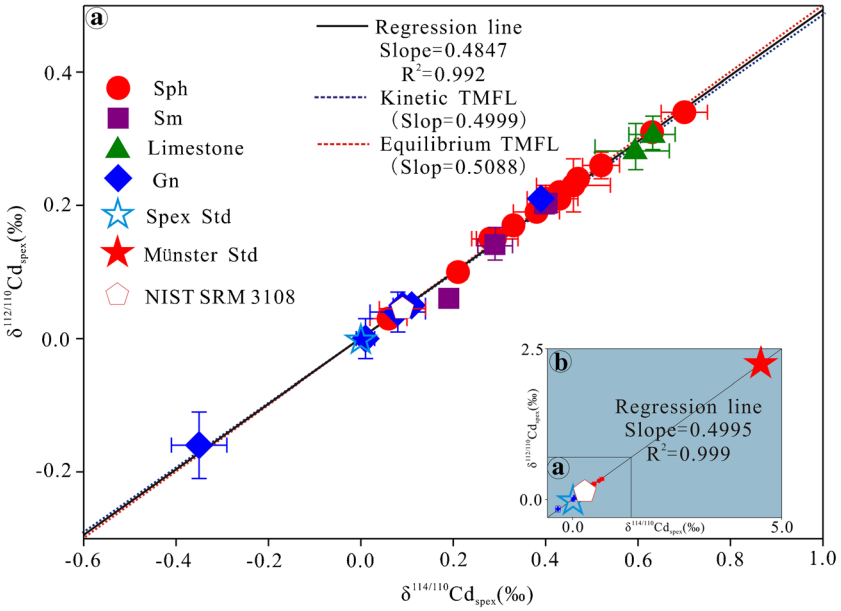

Fig. 5 Plot of $\delta^{114/110}Cd_{spex}$ vs $\delta^{112/110}Cd_{spex}$ for the samples from the Fule deposit. All samples fall within the error of the theoretical mass fractionation line (*TMFL*), including the Cd standards (Spex, NIST 3108, and Münster Cd standard). The slope for the Münster Cd standard and samples for a given session are equal and have the slope of 0.4997 predicted for the theoretical fractionation line. This finding demonstrates (1) the constancy of the analytical mass fractionation and the overall stability of the instrument during sample measurement, (2) all isobaric interference was efficiently removed, and (3) there are no resolvable nucleosynthetic isotopic anomalies at the delta unit scale

Zn ratios of bulk galena samples (from 159 to 512) are within the range of sphalerite samples (23–588). Second, the Cd contents in galena samples are positively correlated with those of Zn ([Cd] = 485 [Zn] + 0.158, r = 0.97, n = 6) (Fig. 8). Third, BSE images confirmed that sphalerite micro-inclusions are present within galena (Figs. 3d, e).

LA-ICP-MS measurements showed direct substitution of Zn^{2+} by Cd^{2+} during crystallization of sphalerite (Cook et al. 2009), whereas Belissont et al. (2014) suggested that Fe and Cd are mainly involved in direct substitution of Zn^{2+} by Cd^{2+} and Fe^{2+}. In the Fule deposit, sphalerite has high Cd contents (5240–35,000 ppm) but low Fe contents (365–970 ppm), suggesting that Cd is mainly related to direct substitution of Zn^{2+} by Cd^{2+}.

Besides the study on the occurrence of Cd in sphalerite, few studies have focused on the Cd substitution mechanisms in smithsonite (Tu et al. 2004). The geochemical behavior of Cd in the supergene environment is similar to that of Zn; Tu et al. (2004) suggested that Cd is probably involved in direct substitution of Zn^{2+} by Cd^{2+}. Back-scattered electron images show that no Cd-independent minerals have been observed in smithsonite of the Fule deposit at the micro scale. Thus, we

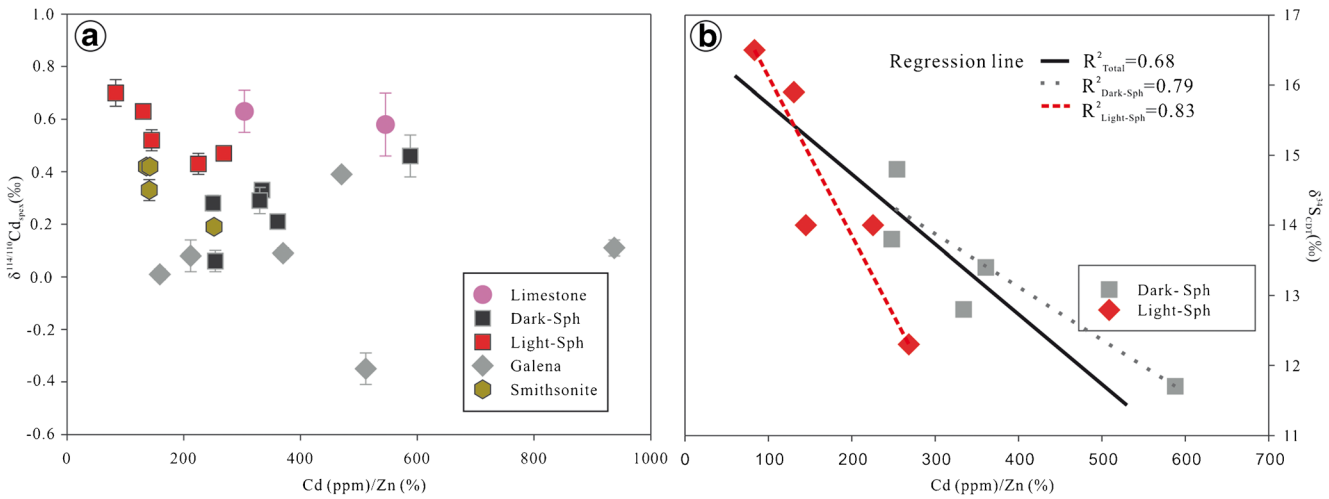

Fig. 6 **a**, **b** Plots of $\delta^{114/110}Cd_{spex}$ vs Cd/Zn ratio for the samples from the Fule deposit

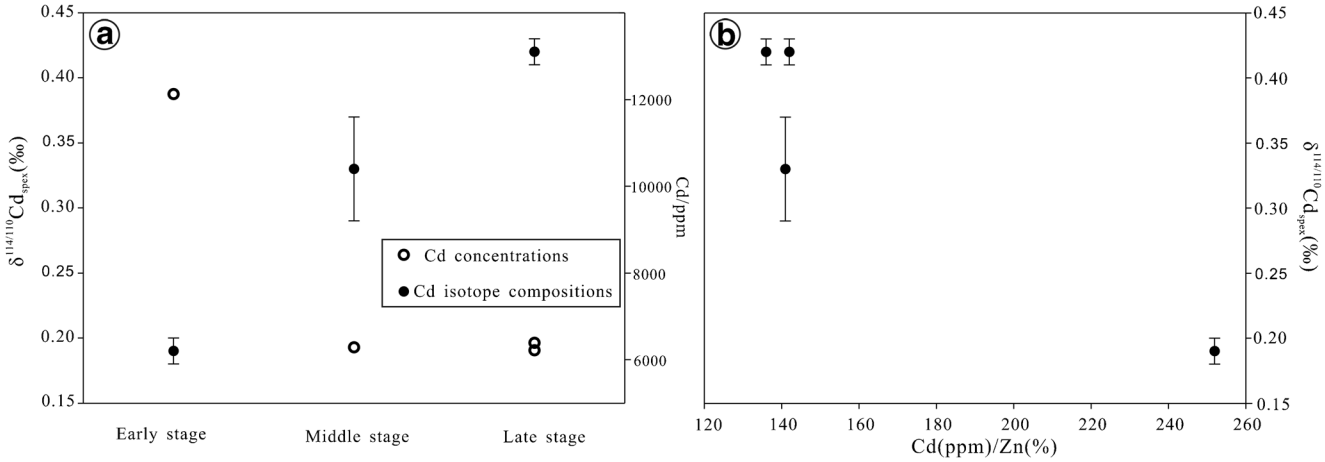

Fig. 7 Diagrams of Cd isotope composition vs Cd abundance (**a**) and vs Cd/Zn ratio (**b**) of early- to late-stage smithsonite

suggest that Cd substitutes for Zn in smithsonite, similar to the substitution of Cd in sphalerite (Cook et al. 2009) and Cd in calcite (Horner et al. 2011).

Cd isotope composition of layered smithsonite

When sphalerite was oxidized, layered smithsonite precipitated from low-temperature fluids in the Fule deposit. As illustrated in Fig. 3f, layered smithsonite shows a clear growth direction. From the early to late precipitation stages, the Cd isotope composition continually becomes heavier with the decrease of Cd contents in smithsonite (Figs. 3f and 7), with $\delta^{114/110}$Cd values ranging from 0.19 to 0.42 ‰, which resembles the trends of Fe and Zn isotopic variations in layered sphalerite from the Navan deposit (Gagnevin et al. 2012). Experimental studies of Horner et al. (2011) show that Cd readily substitutes for Ca during the crystallization of calcite and the Cd isotope fractionation in calcite is controlled by kinetic Rayleigh fractionation. Similarly, Cd readily substitutes for Zn during the crystallization of smithsonite. Thus, it can be concluded that Cd isotope fractionation in smithsonite is also controlled by kinetic Rayleigh fractionation. Yang et al. (2014) calculated the fractionation properties of Cd species in hydrothermal fluids, suggesting that light Cd preferentially partitions into the solid phase rather than the solution. Thus, these findings indicate that the Cd isotopic fractionation during smithsonite precipitation also follows a kinetic Rayleigh fractionation process.

Cadmium isotope composition of sphalerite

From the bottom to the top of the orebody, the Cd/Zn ratios of sphalerite micro-inclusions in galena are similar (Fig. 9a), while the $\delta^{114/110}$Cd values increase with sampling height

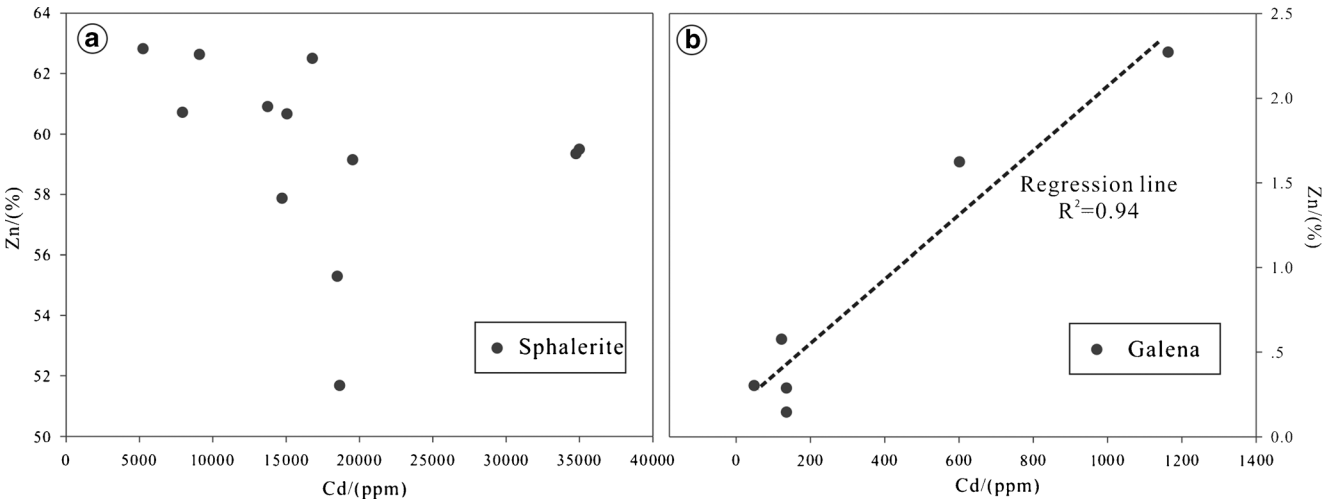

Fig. 8 Plots of Cd vs Zn contents of sphalerite (**a**) and galena (**b**). No strong correlation between Cd and Zn contents of sphalerite is apparent for the entire dataset, but a strong correlation is observed for six galena samples suggesting that Cd in galena is present as sphalerite micro-inclusions

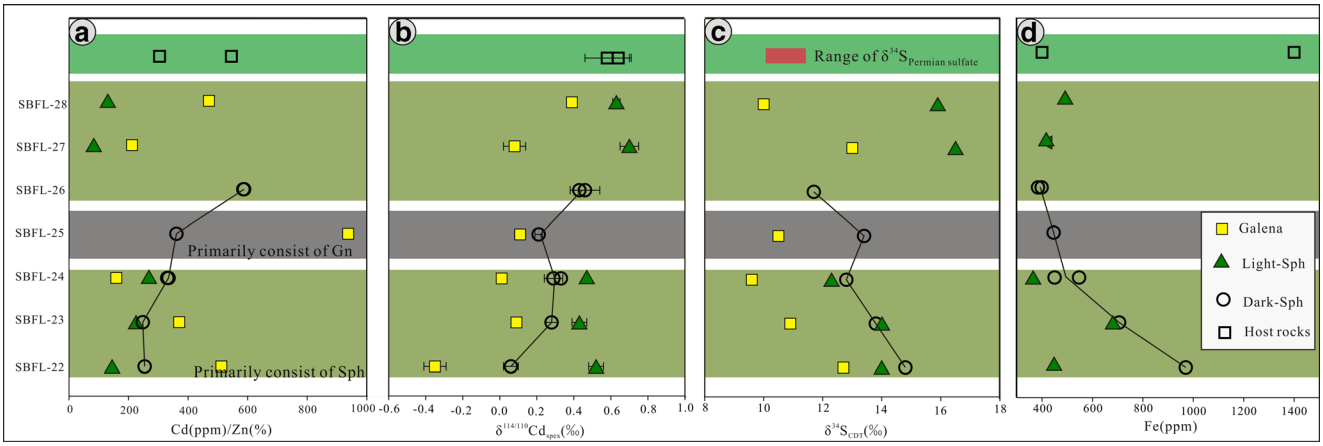

Fig. 9 Cd/Zn ratio (**a**), $\delta^{114/110}$Cd value (**b**), δ^{34}S (**c**), and Fe concentration (**d**) in sulfides and host rocks from the bottom to the top of the studied orebody. The range of δ^{34}S is Permian seawater sulfate (Clayton 1981)

(Fig. 9b). In the dark sphalerite of the same profile, the Cd/Zn ratios and $\delta^{114/110}$Cd values increase regularly from 250 to 590 and 0.06 to 0.46 ‰, respectively, whereas δ^{34}S values and Fe concentrations decrease regularly from 14.8 to 11.7 ‰ and 970 to 400 ppm, respectively (Fig. 9; Table 2). Although the $\delta^{114/110}$Cd values of light sphalerite increase from the bottom to the top of the orebody, Cd/Zn ratios, δ^{34}S values, and Fe have no correlation with sampling height (Fig. 9). Meanwhile, the regression lines of δ^{34}S vs Cd/Zn ratios of dark and light sphalerite are quite different (Fig. 6b). Taken together, these results suggest that dark and light sphalerite is likely deposited under different conditions.

The variation patterns of $\delta^{144/110}$Cd values and Cd/Zn ratios in light sphalerite are similar to that of layered smithsonite (Figs. 6b and 7b). If the interpretation of Cd isotopic composition in layered smithsonite best fits the data available at the present time, the Cd isotopic fractionation during light sphalerite precipitation also follows a kinetic Rayleigh fractionation process. Considering that the geochemical behavior of Cd in Zn–Pb deposits is similar to that of Zn (Metz and Trefry 2000; Schwartz 2000), it is possible that Cd isotopes behave similar to Zn isotopes (Schmitt et al. 2009). The recent study of Gagnevin et al. (2012) demonstrated that the δ^{66}Zn values of six microdrilled sphalerite samples from the Navan deposit, Ireland, increased regularly from early- to late-stage sphalerite, with values from −0.27 to 0.06 ‰, which is similar to the trend of Cd isotopic variations observed in this study (Figs. 4 and 9b). Lighter δ^{66}Zn values have also been reported in black sphalerite from some typical Zn–Pb deposits (Tianqiao, Banbanqiao, and Shanshulin) in the western Yangtze Block, which formed in geological settings similar to that of the Fule deposit (Fig. 2; Zhou et al. 2014a, b). Gagnevin et al. (2012) suggested that the Zn isotopes in the Navan deposit had primarily undergone kinetic fractionation during rapid sphalerite precipitation, which resulted in lighter δ^{66}Zn values in the early-stage sphalerite. Zhou et al. (2014a, b) also suggested that the Zn isotopic fractionation among different-colored sphalerite domains can be explained by kinetic Rayleigh fractionation. Moreover, Horner et al. (2011) confirmed that Cd readily substitutes for Ca during the crystallization of calcite, which is controlled by a kinetic Rayleigh fractionation process, and is similar to the substitution of Zn by Cd during sphalerite crystallization. Thus, the kinetic Rayleigh fractionation model might be the best explanation for Cd fractionation in light sphalerite at the present time.

The trend lines of $\delta^{144/110}$Cd vs Cd/Zn and $\delta^{144/110}$Cd vs δ^{34}S of dark sphalerite are quite different from those of the light one (Figs. 9a–c), indicating that the fractionation mechanisms of Cd and S isotopes are different in dark and light sphalerite. Previous studies have shown that the negative relationships between δ^{66}Zn and δ^{34}S in sphalerite can be explained by mixing of Zn from two sources (Wilkinson et al. 2005). Gagnevin et al. (2012) also suggested that fluid mixing could result in negative relationships between δ^{66}Zn and δ^{34}S in sphalerite. Similarly, we suggest that the relationship between $\delta^{144/110}$Cd and δ^{34}S and between $\delta^{144/110}$Cd and Cd/Zn of dark sphalerite could be modeled in terms of two-component mixing.

Sulfur isotope composition of primary ores

There is usually little temperature variation (70–170 °C) in typical MVT deposits (Leach et al. 2005). However, based on the published equation for sphalerite–galena pairs (Clayton 1981), the calculated temperatures at Fule decreased from 328 to 86 °C towards the top of the studied orebody, which are much higher than in typical MVT deposits. This result indicates that the δ^{34}S values in galena and sphalerite at Fule are not in equilibrium in the S isotopic system and cannot be used as geothermometers.

In the SYG area, an increase of δ^{34}S values in sphalerite sampled from bottom to top of the orebody has been observed in the Huize deposit (8 to 14 ‰) (Huang et al. 2004), which is similar to the variation of δ^{34}S values in light sphalerite at

Fule. However, a decrease of $\delta^{34}S$ values in sphalerite sampled from early to late sphalerite stages (15 to 11 ‰) has been reported in the Tianqiao deposit (Zhou et al. 2014a), which is similar to the variation of $\delta^{34}S$ values in dark sphalerite. These findings indicate that the variation of S isotopes in different deposits may be controlled by different processes. Previous studies have shown that the increase of $\delta^{34}S$ values can be explained by cooling of a single hydrothermal fluid because the $\delta^{34}S$ values of sulfides increase with cooling (Rye and Ohmoto 1974; Thiessen et al. 2016). However, decreasing $\delta^{34}S$ values can also be explained by fluid mixing processes, which have been considered as the explanation for the decrease of $\delta^{34}S$ values in sulfides from the Bluebell deposit (Rye and Ohmoto 1974). Bortnikov et al. (1995) also suggested that fluid mixing may have caused the temporal and spatial variations in $\delta^{34}S$ values of sulfides from the Karamazar Cu–Bi–Ag–Pb deposits, Middle Asia. Combined with the Cd isotopic data, it can be concluded that S in the Fule deposit was possibly derived from the mixing of sulfur from Permian host rocks ($\delta^{34}S_{Permian\text{-}sulfate}$ = 10–15 ‰; Claypool et al. 1980) and basement rocks ($\delta^{34}S_{Precambrian\ sulfate}$ = 15–35 ‰; Claypool et al. 1980), and most of the reduced S in the sulfides was derived from the host rocks (Si 2005).

However, factors that control the sulfur isotopic composition of hydrothermal minerals are complex, including temperature, oxygen fugacity, pH, and relative amount of the mineral precipitated from the fluids (Rye and Ohmoto 1974; Zheng and Hoefs 1993; Bortnikov et al. 1995), which should be taken into account for a more detailed explanation of the $\delta^{34}S$ values in the Fule Zn–Pb deposit.

Conclusions

(1). An increasing trend in the $\delta^{114/110}Cd$ isotope composition and Cd/Zn ratio of layered smithsonite from early to late stages was observed, which can be explained by kinetic Rayleigh fractionation.

(2). Sphalerite is the primary Cd-bearing mineral in the Fule Zn–Pb deposit, while galena is not. Cadmium isotopic data reported for bulk galena samples are controlled by their sphalerite micro-inclusions.

(3). The $\delta^{114/110}Cd$ isotope compositions, Cd/Zn ratios, $\delta^{34}S$ values, and Fe concentrations of sphalerite show different systematic variations in dark and light sphalerite from the bottom to the top of the orebody, indicating that dark and light sphalerite precipitated from different hydrothermal processes.

(4). Comparison of the light sphalerite and layered smithsonite shows an increasing trend in $\delta^{114/110}Cd$ value and Cd/Zn ratio in both minerals, indicating that Cd fractionation in light sphalerite can be explained by kinetic Rayleigh fractionation. The decrease of $\delta^{34}S$ values in light sphalerite may be caused by cooling of a single hydrothermal fluid.

(5). Cd and S isotope fractionation in dark sphalerite can be explained by two-component fluid mixing.

Acknowledgments This work was financially supported by National Natural Science Foundation of China (Nos. 41503011, 41573007, 40930425, and 41173026), the Strategic Priority Research Program of CAS (XDB18030302), 973 Program (2014CB440904), CAS/SAFEA International Partnership Program for Creative Research Teams (No. KZZD-EW-TZ-20) and CAS "Light of West China".

References

Belissont R, Boiron MC, Luais B, Cathelineau M (2014) LA-ICP-MS analyses of minor and trace elements and bulk Ge isotopes in zoned Ge-rich sphalerites from the Noailhac–Saint-Salvy deposit (France): insights on incorporation mechanisms and ore deposition processes. Geochim Cosmochim Acta 126:518–540

Bortnikov NS, Dobrovol'skaya MG, Genkin AD, Naumov VB, Shapenko VV (1995) Sphalerite-galena geothermometers; distribution of cadmium, manganese, and the fractionation of sulfur isotopes. Econ Geol 90:155–180

Claypool GE, Holser WT, Kaplan IR, Sakai H, Zak I (1980) The age curves of sulfur and oxygen isotopes in marine sulfate and their mutual interpretation. Chem Geol 28:199–260

Clayton RN (1981) Isotopic thermometry. In: Newton RC, Navrotsky A, Wood BJ (eds) Thermodynamics of minerals and melts. Springer Verlag, New York, pp. 85–109

Cloquet C, Rouxel O, Carignan J, Libourel G (2005) Natural cadmium isotopic variations in eight geological reference materials (NIST SRM 2711, BCR 176, GSS-1, GXR-1, GXR-2, GSD-12, Nod-P-1, Nod-A-1) and anthropogenic samples, measured by MC-ICP-MS. Geostandard Geoanal Res 29:95–106

Cloquet C, Carignan J, Libourel G, Sterckeman T, Perdrix E (2006) Tracing source pollution in soils using cadmium and lead isotopes. Environ Sci Technol 40:2525–2530

Cook NJ, Ciobanu CL, Pring A, Skinner W, Shimizu M, Danyushevsky L, Saini-Eidukat B, Melcher F (2009) Trace and minor elements in sphalerite: a LA-ICPMS study. Geochim Cosmochim Acta 73: 4761–4791

Gagnevin D, Boyce AJ, Barrie CD, Menuge JF, Blakeman RJ (2012) Zn, Fe and S isotope fractionation in a large hydrothermal system. Geochim Cosmochim Acta 88:183–198

Han RS, Liu CQ, Huang ZL, Chen J, Ma DY, Lei L, Ma GS (2007) Geological features and origin of the Huize carbonate-hosted Zn–Pb–(Ag) district, Yunnan, South China. Ore Geol Rev 31:360–383

Horner TJ, Rickaby REM, Henderson GM (2011) Isotopic fractionation of cadmium into calcite. Earth Planet Sci Lett 312:243–253

Huang ZL, Chen J, Han RS, Li WB, Liu CQ, Zhang ZL, Ma DY, Gao DR, Yang ML (2004) Geochemistry and ore-formation of the Huize giant lead-zinc deposit, Yunnan Province, China: discussion on the relationship between Emeishan flood basalts and lead-zinc mineralization (in Chinese). Geological Publishing House, Beijing, pp. 50–146

Lambelet M, Rehkämper M, Flierdt T, Xue ZC, Kreissig K, Coles B, Porcelli D, Andersson P (2013) Isotopic analysis of Cd in the mixing zone of Siberian rivers with the Arctic Ocean—new constraints on marine Cd cycling and the isotope composition of riverine Cd. Earth Planet Sci Lett 361:64–73

Leach DL, Sangster DF, Kelley KD, Large RR, Garven G, Allen CR, Gutzmer J, Walters S (2005) Sediment-hosted lead-zinc deposits: a global perspective. In: Hedenquist JW, Thompson JFH, Goldfarb

RJ, Richards JP (eds) Economic geology 100th anniversary volume. Society of Economic Geologists, Littleton, pp. 561–607

Liu J, Wen HJ, Zhang YX, Fan HF, Zhu CW (2016) Precise Mo isotope ratio measurements of low-Mo (ng g^{-1}) geological samples using MC-ICP-MS. J Analyt Atomic Spectrom. doi:10.1039/C6JA00006A

Metz S, Trefry JH (2000) Chemical and mineralogical influences on concentrations of trace metals in hydrothermal fluids. Geochim Cosmochim Acta 64:2267–2279

Palero-Fernández FJ, Martín-Izard A (2005) Trace element contents in galena and sphalerite from ore deposits of the Alcudia Valley mineral field (Eastern Sierra Morena, Spain). J Geochem Explor 86:1–25

Pallavicini N, Engstrom E, Baxter DC, Ohlander B, Ingri J, Rodushkin I (2014) Cadmium isotope ratio measurements in environmental matrices by MC-ICP-MS. J Analyt Atomic Spectrom 29:1570–1584

Ripperger S, Rehkämper M, Porcelli D, Halliday AN (2007) Cadmium isotope fractionation in seawater—a signature of biological activity. Earth Planet Sci Lett 261:670–684

Rudnick RL, Gao S (2003) Composition of the continental crust. Treatise Geochem 3:1–64

Rye RO, Ohmoto H (1974) Sulfur and carbon isotopes and ore genesis: a review. Econ Geol 69:826–842

Schmitt AD, Stephen JG, Abouchami W (2009) Mass-dependent cadmium isotopic variations in nature with emphasis on the marine environment. Earth Planet Sci Lett 277:262–272

Schwartz MO (2000) Cadmium in zinc deposits: economic geology of a polluting element. Int Geol Rev 42:445–469

Si RJ (2005) Ore deposit geochemistry of the Fule dispersed element-polymetallic deposit, Yunnan Province. A dissertation submitted to Chinese Academy of Sciences for a doctor degree. Guiyang (In Chinese with English abstract)

Thiessen EJ, Gleeson SA, Bennett V, Creaser RA (2016) The Tiger deposit: a carbonate-hosted, magmatic-hydrothermal gold deposit, Central Yukon, Canada. Econ Geol 111:421–446

Tu GC, Gao ZM, Hu RZ, Zhang Q, Li CY, Zhao ZH, Zhang BG (2004) The geochemistry and deposit-forming mechanism of disperse elements. Geological Publishing House, Beijing, pp. 69–115 in Chinese

Wen HJ, Zhang YX, Cloquet C, Zhu CW, Fan HF, Luo CG (2015) Tracing sources of pollution in soils from the Jinding Pb–Zn mining district in China using cadmium and lead isotopes. Appl Geochem 52:147–154

Wen HJ, Zhu CW, Zhang YX, Cloque C, Fan HF, Fu SH (2016) Zn/Cd ratios and cadmium isotope evidence for the classification of lead-zinc deposits. Sci Rep. doi:10.1038/srep25273

Wilkinson JJ, Weiss DJ, Mason TFD, Coles BJ (2005) Zinc isotope variation in hydrothermal systems: preliminary evidence from the Irish midlands ore field. Econ Geol 100:583–590

Wombacher F, Rehkämper M, Mezger K, Münker C (2003) Stable isotope compositions of cadmium in geological materials and meteorites determined by multiple-collector ICP-MS. Geochim Cosmochim Acta 23:4639–4654

Yang JL, Li YB, Liu SQ, Tian HQ, Chen CY, Liu JM, Shi YL (2014) Theoretical calculations of Cd isotope fractionation in hydrothermal fluids. Chem Geol 391:74–82

Ye L, Cook NJ, Ciobanu CL, Liu YP, Zhang Q, Liu TG, Gao W, Yang YL, Danyushevskiy L (2011) Trace and minor elements in sphalerite from base metal deposits in South China: a LA-ICPMS study. Ore Geol Rev 39:188–217

Zhang YX, Wen HJ, Zhu CW, Fan HF, Luo CG, Liu J, Cloquet C (2016) Cd isotope fractionation during simulated and natural weathering. Environ Pollut 216:9–17

Zheng YF, Hoefs J (1993) Effects of mineral precipitation on the sulfur isotope composition of hydrothermal solutions. Chem Geol 105:259–269

Zhou JX, Huang ZL, Zhou GF, Li XB, Ding W, Bao GP (2011) Trace elements and rare earth elements of sulfide minerals in the Tianqiao Pb-Zn ore deposit, Guizhou Province China. Acta Geol Sin (English Edition) 85:189–199

Zhou JX, Huang ZL, Zhou MF, Li XB, Jin ZG (2013) Constraints of C-O-S-Pb isotope compositions and Rb-Sr isotopic age on the origin of the Tianqiao carbonate–hosted Pb–Zn deposit, SW China. Ore Geol Rev 53:77–92

Zhou JX, Huang ZL, Zhou MF, Zhu XK, Muchez P (2014a) Zinc, sulfur and lead isotopic variations in carbonate-hosted Pb-Zn sulfide deposits, southwest China. Ore Geol Rev 58:41–54

Zhou JX, Huang ZL, Lv ZC, Zhu XK, Gao JG, Mirnejad H (2014b) Geology, isotope geochemistry and ore genesis of the Shanshulin carbonate-hosted Pb-Zn deposit, southwest China. Ore Geol Rev 63: 209–225

Zhu CW, Wen HJ, Zhang YX, Fan HF, Fu SH, Xu J, Qin TR (2013) Characteristics of Cd isotopic compositions and their genetic significance in the lead-zinc deposits of SW China. Sci China Earth Sci 56:2056–2065

Zhu CW, Wen HJ, Zhang YX, Liu YZ, Wei RF (2015) Isotopic geochemistry of cadmium: a review. Acta Geol Sinica (English Edition) 89: 2048–2057

Zhu CW, Wen HJ, Zhang YX, Fan HF (2016) Cadmium and sulfur isotopic compositions of the Tianbaoshan Zn-Pb-Cd deposit, Sichuan Province, China. Ore Geol Rev 76:152–162